Applied Catalysis A: General 469 (2014) 1–7

Contents lists available at ScienceDirect

Applied Catalysis A: General

journal homepage: www.elsevier.com/locate/apcata

Calcination effects on $CeZrO_x$ geometry and styrene production from ethylbenzene

M. Kovacevic, R. Brunet Espinosa, L. Lefferts, B.L. Mojet*

Catalytic Processes and Materials, Faculty of Science and Technology, MESA+ Institute for Nanotechnology, University of Twente, P.O. Box 217, 7500 AE Enschede, The Netherlands

ARTICLE INFO

Article history:
Received 19 April 2013
Received in revised form 4 September 2013
Accepted 9 September 2013
Available online 19 September 2013

Keywords:
Ethylbenzene dehydrogenation
Doped-ceria
Morphology change

ABSTRACT

A series of $CeZrO_x$ catalysts was prepared by calcination of hydrothermally obtained metal oxide precipitate at increasing temperatures. The samples were characterized by HRSEM, XRD and Raman spectroscopy, showing a change in morphology and particle size as a function of calcination temperature. Catalytic testing for ethylbenzene dehydrogenation with CO_2 showed a decreasing activity per gram with increasing calcination temperature due to the decreasing particle size. However, ethylbenzene dehydrogenation activity per m^2 also steadily decreased. Correlation of the catalytic results with Raman analysis showed that not only the number of oxygen vacancies decreases with increasing particle size due to a lower surface area, but also their specific reactivity decreased because of a change in the particle morphology.

1. Introduction

Cerium oxide is a key compound for various applications, like gas sensors [1,2], solid oxide fuel cells [3–5] and solar cells [6,7]. Ceria based catalysts are useful for automobile exhaust treatments [8,9], CO oxidation [10,11], low temperature water-gas-shift reaction [12,13] and CO_2 activation [14].

Recently, cerium oxide was also reported being a promising catalyst for ethylbenzene dehydrogenation (EBDH) in the presence of oxygen [15] or N_2O [16]. EBDH for the production of styrene has attracted lots of attention lately, attempting to minimize energy consumption of the process [17,18]. The route to styrene using carbon dioxide as a soft oxidant, which can replace conventionally used steam, has been initially suggested back in the 1990s by various research groups [19–22]. CO_2 addition requires less dilution compared to steam due to its high heat capacity. CO_2 is proposed to increase ethylbenzene equilibrium conversion due to the reverse water gas shift (RWGS) [23,24] reaction. Moreover, CO_2 has been suggested to turn the reaction pathway to an oxidative route enhancing the reaction rate [18,21]. In addition, CO_2 possibly prolongs catalyst life time by coke gasification via the Boudart reaction. Bulk V/MgO catalyst, for instance, produces 2.5 times higher amount of styrene in the presence of CO_2 compared to Ar atmosphere [25]. Carbon supported vanadia based catalysts are reported as promising candidates for EBDH with CO_2, however strong deactivation due to coke deposition occurred [26]. Coke deposits on the other hand were reported as catalytically active for EBDH in the presence of CO_2 for alumina and zirconia catalysts [27].

The role of acid–base and redox properties together with the activity of surface/ lattice oxygen species in EBDH with CO_2 have been extensively discussed by the group of Park for various catalytic systems [18]. An earlier comprehensive study suggested mixed ZrO_2 based oxides as highly suitable for EBDH with CO_2 [28]. An increasing catalytic activity from pure oxides, to mixed oxides and finally mixed oxide supported on SBA-15 was also reported [29].

Pure ceria was reported to have an extraordinary oxygen storage capacity (OSC) which was proposed to explain the unique catalytic properties [30]. The OSC of ceria is related to the oxygen vacancy concentration that in turn depends on catalyst morphology, shape, crystallite size and calcination history of the material [31]. The oxygen vacancy concentration of ceria can be enhanced by the addition of a modifier, such as lower valence metal cations [32]. Doping with iso-valent Zr^{4+} was also reported to increase oxygen deficiency and reducibility of ceria [33–35]. Further, it was reported that increasing calcination temperature induces defect annihilation in pure ceria [36], while for zirconia–ceria solid solutions ageing at 850 °C hardly affect the oxygen storage capacity [32]. The aim of the present study is to explore the properties of cubic shaped zirconia doped ceria for EBDH with CO_2. Ceria cubes have specifically different surface planes (1 0 0) exposed than generally applied polycrystalline CeO_2 (1 1 1) [37,38] and have a high intrinsic oxygen defect stability. The effect of calcination temperature on the structure and defect concentration of a series of $CeZrO_x$ catalysts is investigated and related to the catalytic activity for EBDH with CO_2.

* Corresponding author. Tel.: +31 53 489 2999; fax: +31 53 489 4683.
E-mail address: B.L.Mojet@Utwente.nl (B.L. Mojet).

0926-860X/$ – see front matter © 2013 Elsevier B.V. All rights reserved.
http://dx.doi.org/10.1016/j.apcata.2013.09.010

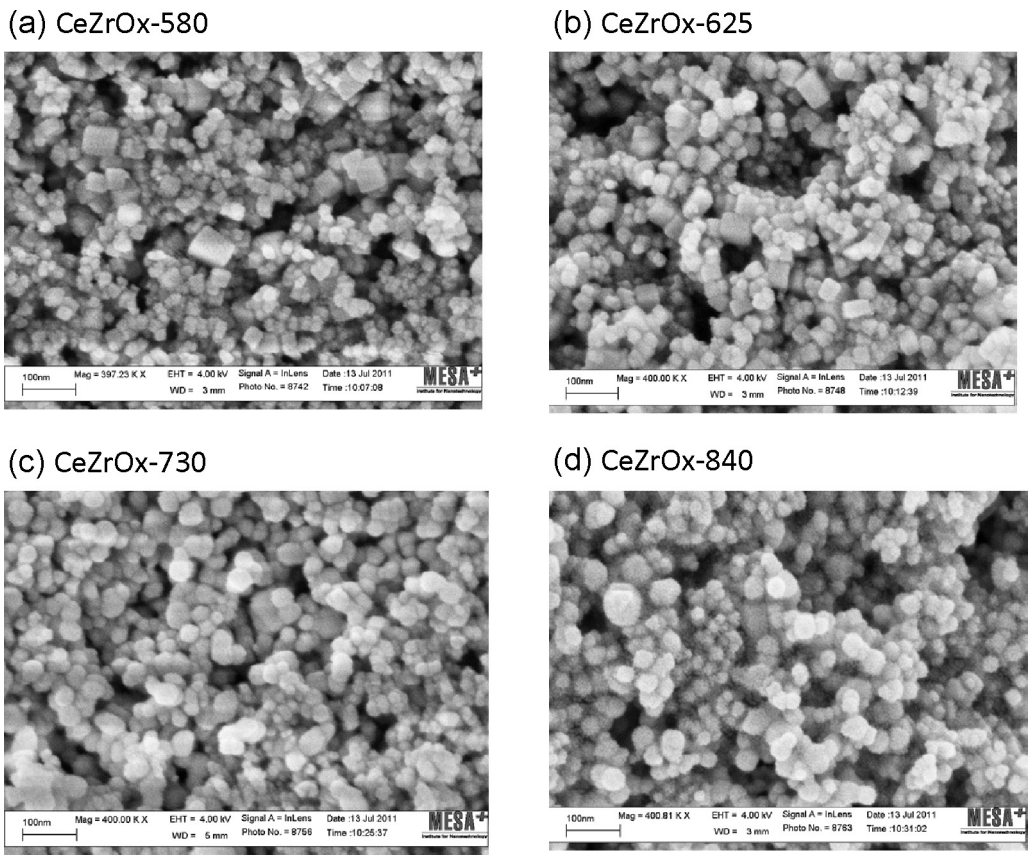

Fig. 1. HRSEM images: $CeZrO_x$-580 (a), $CeZrO_x$-625 (b), $CeZrO_x$-730 (c) and $CeZrO_x$-840 (d) catalysts.

2. Experimental

2.1. Materials

Commercially available NaOH pellets (Merck, 99%), $Ce(NO_3)_3{\cdot}6H_2O$ (99.99% Aldrich) and monoclinic ZrO_2 (Magnesium Electron Ltd., MEL, BET surface area is 3 $m^2\,g^{-1}$) were used for catalyst synthesis.

2.2. Catalyst preparation

A series of $CeZrO_x$ catalysts was prepared following the hydrothermal synthesis procedure described elsewhere [39]. We used an autoclave of 125 mL volume keeping the rest of the experimental conditions identical to the procedure in Ref. [39]. In short, a NaOH solution was prepared diluting 110 g of NaOH in 170 mL of deionized water. In parallel, 1 g of $Ce(NO_3)_3{\cdot}6H_2O$ and 0.025 g of ZrO_2 was dispersed in 17 mL of deionized water. The two solutions were mixed and stirred (250 rpm) for 10 min. Finally, 20 mL of deionized water was added to the resulting mixture, which was transferred to an autoclave and hydrothermally heated at 150 °C for 19 h. The obtained precipitate was dried at 110 °C overnight (static air), divided into four portions and calcined in flowing artificial air (5 h, 50 mL min^{-1}). The series of $ZrCeO_2$ catalysts (molar ratio Ce:Zr = 92:8) are denoted as: $CeZrO_x$-580, $CeZrO_x$-625, $CeZrO_x$-730 and $CeZrO_x$-840 with the number indicating the respective calcination temperature. It should be noted that by this preparation procedure cubic shaped particles were obtained, contrary to the rod shaped particles described in the Ref. [39].

A reference pure ceria sample, CeO_2-625, was prepared following the same preparation route, but without addition of ZrO_2, and subsequently calcined at 625 °C. Pure monoclinic ZrO_2 was calcined at 625 °C prior to reaction as a second reference sample.

2.3. Catalyst characterization

Catalyst surface area (BET) was determined by N_2-adsorption at 77 K (Micromeritics Tristar). The samples were out-gassed in vacuum at 200 °C for 24 h prior to analysis.

Sample morphology was studied by scanning electron microscopy (LEO 1550 FEG-HRSEM) equipped with an in-lens detector.

X-ray diffraction (XRD) patterns were recorded using a Bruker D2 powder diffractometer equipped with a position sensitive detector over a 2θ-range between 15° and 75° using Cu Kα radiation, $\lambda = 0.1544$ nm. The average crystallite size was determined based on X-ray line broadening using Scherrer's equation.

Raman spectroscopy measurements were performed with a Senterra Bruker instrument, equipped with a cooled CCD detector. The spectra were recorded at $\lambda_{ex} = 532$ nm, 2 s integration time, 20 co-additions, 10 mW laser power and 9–15 cm^{-1} resolution. The quantification of species was performed on baseline corrected spectra normalized to the intensity of the peak at 464 cm^{-1} taking the tailing of the main peak into account.

Thermal gravimetric analysis (TG, Mettler Toledo), was conducted in flowing artificial air. Typically 10 mg of sample was dried at 125 °C for 30 min and cooled to room temperature. Subsequently, temperature increased to 800 °C with 10 °C min^{-1} ramp.

2.4. Catalytic testing

Catalytic tests were carried out at atmospheric pressure at 560 °C in a fixed-bed quartz tubular reactor (4.0 mm i.d.). The

Table 1
Nitrogen physisorption and crystallite size (from XRD).

Catalyst	S_{BET} ($m^2\ g^{-1}$)	Crystallite size (nm)
ZrO_2	3	n.d.
CeO_2-625	35	n.d.
$CeZrO_x$-580	36	24
$CeZrO_x$-625	34	25
$CeZrO_x$-730	32	32
$CeZrO_x$-840	28	41

amount of catalyst per run was tuned in such a way that ethylbenzene (EB) conversion reached 6 ± 2% stable differential level after approximately 120 min time-on-stream. EB concentration in the gas phase was controlled at 1 mol% via the vapour pressure using a double saturator. In the first saturator EB was evaporated at 35 °C, followed by condensation at 23 °C in the second saturator. CO_2 was added as a soft oxidant and CO_2 to EB ratio was adjusted to 7 in a total flow of 30 ml min^{-1} (balance N_2). Prior to reaction, catalysts were pretreated in pure N_2 at 580 °C (30 min) and subsequently in CO_2 at the reaction temperature for 30 min. Carbon dioxide is known to interact with ceria quite strongly to form stable carbonates [40]. For this reason the catalysts were treated with CO_2 prior to exposure to ethylbenzene.

Reaction products were analyzed by on-line GC Varian-450 equipped with TCD and FID detector and four columns: Hayesep T, Hayesep Q, Molsieve 13X and CP-Wax The experiments were reproducible with a typical overall error of ±5%.

Catalyst activity is expressed as the amount of EB or carbon dioxide converted per weight of catalyst or catalyst surface area. Selectivity to styrene ($Sel._{Sty}$) is defined as the fraction of styrene to the total aromatics' content (Eq. (1)).

$$Sel._{Sty}(\%) = \frac{\text{Styrene}}{\text{Styrene} + \text{Toluene} + \text{Benzene}} \times 100\% \quad (1)$$

The carbon balance was calculated as the ratio of the sum of all aromatic compounds in product stream (styrene, toluene, benzene and non-reacted EB) vs. the amount of EB being fed to the reactor. CO_2 was not taken into account for the carbon balance because of its low conversion and thus extremely high contribution to the overall carbon-balance. The carbon balance based on aromatics varied between 98.2% and 99.5%.

3. Results

3.1. Catalyst characterization

Fig. 1 shows the HRSEM images of the $CeZrO_x$ samples after calcination at different temperatures. The catalysts' morphology clearly changed with increasing calcination temperature as can be seen from the HRSEM images in Fig. 1a–d. After calcination at 580 °C (Fig. 1a), the $CeZrO_x$ particles had a regular cubic shape. With increasing calcination temperature, the catalyst particles became more rounded and transformed into spherical shapes after calcination at 840 °C. In addition, the $CeZrO_x$ particle size increased with increasing calcination temperature.

Fig. 2 shows the X-ray diffraction (XRD) patterns of $CeZrO_x$ catalysts calcined at 580–840 °C. For all investigated samples dominant Bragg diffractions were observed at 28.8°, 47.6° and 56.7° 2θ, corresponding to respectively (1 1 1), (2 2 0) and (3 1 1) crystal planes of the fluorite fcc structure of CeO_2 [41]. Very weak Bragg diffractions at 31.2° and 34.2° correspond to monoclinic zirconia phase [42]. Table 1 summarizes the particle size as calculated from the peak widths in the XRD plots.

Nitrogen physisorption showed a gradual decrease in BET surface area with increasing calcination temperature (Table 1).

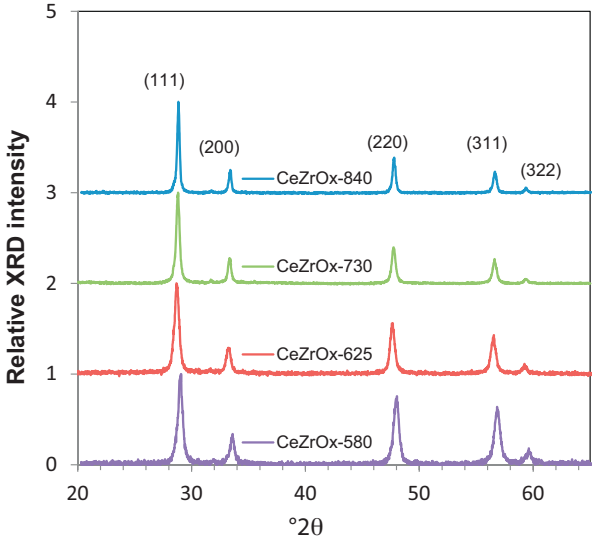

Fig. 2. XRD patterns of $CeZrO_x$ catalysts calcined at 580–840 °C.

Raman spectroscopy was used to further investigate the catalyst structure. Fig. 3a shows the normalized Raman spectrum of $CeZrO_x$-625 as a typical example for the studied samples together with the spectrum of pure CeO_2-625 and monoclinic ZrO_2 (not normalized). The ceria spectra are dominated by a strong peak at 464 cm^{-1} from the F_{2g} mode of the CeO_2 fluorite lattice [43]. Additionally, three weaker bands were identified, assigned to oxygen displacement (258 cm^{-1}), oxygen vacancies (600 cm^{-1}) and lattice oxygen (1170 cm^{-1}) [44]. For CeO_2-625 an additional band is observed around 900 cm^{-1}, which is absent in $CeZrO_x$-625. For $CeZrO_x$-625, the bands from monoclinic zirconia [45] are superimposed on the ceria peaks, suggesting only partial incorporation of zirconia in the ceria lattice.

Fig. 3b shows that upon increasing calcination temperature the width of the F_{2g} band (464 cm^{-1}) steadily decreases. Further, with increasing calcination temperature the peaks at 258 cm^{-1} and between 550 and 650 cm^{-1} clearly decreased.

3.2. Catalytic testing

The $CeZrO_x$ catalysts were tested for ethylbenzene (EB) dehydrogenation with CO_2 as a soft oxidant aiming at differential conversion in steady state after 240 min time on stream (TOS). Typical conversion profiles for EB and CO_2 and product selectivity are shown in Fig. 4. Both EB and CO_2 conversion sharply declined in a similar manner during the initial 120 min (Fig. 4a, and Fig. 1 in supplementary information). The catalysts show similar deactivation patters for EB and CO_2 conversion. The main product of EB dehydrogenation with CO_2 was styrene. During deactivation the selectivity to styrene increased at the expense of the production of benzene and toluene. The selectivity to styrene slowly decreased after the initial increase. At the same time a small, but steady increase of benzene production was observed to approximately 5% after 240 min TOS, at which point all catalysts exhibited about 92 ± 2% selectivity towards styrene (Fig. 4b). The aromatic carbon balance varied between 98.2% and 99.5%. TGA experiments on the spent catalysts confirmed that the missing amount of carbon can be attributed to catalyst coking. Typically, 2–3 wt.% of carbonaceous deposits were found on the spent catalysts.

In steady state, for all catalysts the ratio of [mol CO_2 converted/mol CO produced] equaled 1. Further, the detected amount of produced H_2 was about 40% of the observed amount of styrene.

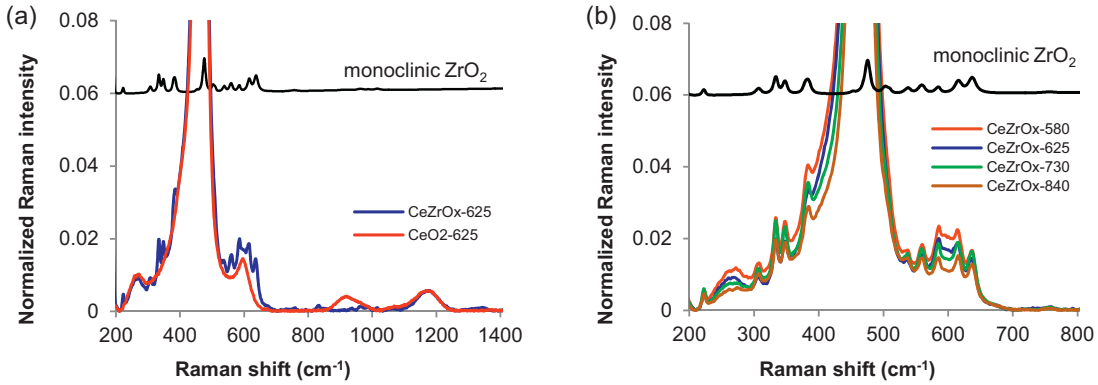

Fig. 3. Typical Raman spectra of (a) $CeZrO_x$-625 (blue), CeO_2-625 (red) and monoclinic ZrO_2 (black); (b) the effect of the calcination temperature on oxygen displacement (258 cm^{-1}), oxygen vacancy (600 cm^{-1}) and ceria F_{2g} (464 cm^{-1}) vibrations of $CeZrO_x$ catalysts. (For interpretation of the references to colour in this figure legend, the reader is referred to the web version of this article.)

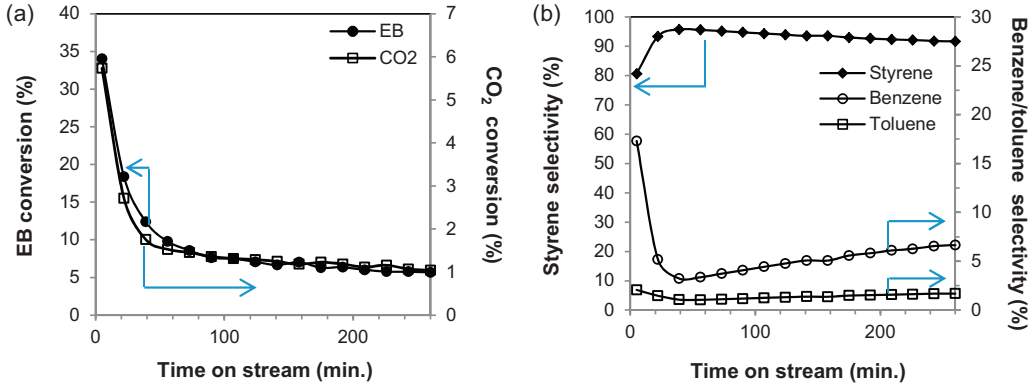

Fig. 4. Testing results for $CeZrO_x$-625 in EBDH with CO_2 as a typical example for all catalysts. Reaction conditions: T = 560 °C, F = 30 ml min^{-1}, CO_2:EB = 7, m_{cat} = 30 mg. (a) Conversion pattern for EB (filled cycles) and CO_2 (empty squares) and (b) corresponding aromatic product selectivity.

Fig. 5 shows the conversion of CO_2 and EB at 240 min TOS per gram of catalyst (a and b) and per m^2 BET surface area (c and d). The conversions obtained with pure CeO_2-625 and monoclinic ZrO_2-625 are given as well. Comparing CeO_2-625 (dashed bar) with $CeZrO_x$-625 indicates a positive effect on the conversion due to the presence of zirconia in the sample. The conversion of EB over pure monoclinic ZrO_2-625 was approximately 5% of the conversion found for the $ZrCeO_2$ samples, while CO_2 conversion was only 3% (based on the amount of ZrO_2 in the samples). Thus, the increase of conversion for $CeZrO_x$-625 is not only due to the possible presence of a ZrO_2 rich phase (monoclinic zirconia) in the sample. Moreover, monoclinic zirconia has been reported as not particular active for the reaction [46]. On the other side, it has been reported that mixed oxides exhibit higher catalytic activity for EBDH with CO_2 compared to their constituent single oxides [28,29].

Increasing calcination temperature led to decreasing EB and CO_2 conversion per gram for the $CeZrO_x$ samples (Fig. 5a and b). Strikingly, when normalized per surface area, the activity per m^2 showed a clear decline with higher calcination temperature (Fig. 5c and d), indicating that the decreasing activity per gram cannot solely be attributed to the decreasing surface area.

4. Discussion

4.1. The effect of calcination temperature on ceria structure

The ex situ characterization of the catalysts by HRSEM (Fig. 1), XRD (Fig. 2, Table 1) and BET (Table 1) confirms an increase of particle size and a decrease of surface area with increasing calcination temperature. In addition, the cubic geometry of the catalyst particles converts into a more spherical shape as was observed in the HRSEM pictures. Both XRD and Raman show the presence of small amounts of monoclinic ZrO_2 in the samples, but the amount could not be calculated because of the very low intensity in the XRD plots.

In the Raman spectra (Fig. 3) the F_{2g} band at 464 cm^{-1} was initially broad and asymmetric for $CeZrO_x$-580, but became narrower and more symmetric with increasing calcination temperature. In literature this peak narrowing has been attributed to annihilation of oxygen vacancies in the fluorite lattice [47], which was confirmed by the simultaneous decrease of the O-displacement band at 258 cm^{-1}. Because of the superposition of the zirconia bands on the oxygen vacancy band at 600 cm^{-1} it is not possible to uniquely assign the decreasing intensity to a decrease in oxygen vacancies, although this may be suggested based on the decrease of the O-displacement band 258 cm^{-1}.

Thermodynamic calculations predict that ceria shape alteration from cubic to spherical particles favours the exposure of (1 1 1) crystal planes at the catalysts surface reducing the number of crystal point defects [31]. The morphology transition of the catalysts with increasing calcination temperature as presented in Fig. 1, thus is expected to decrease the oxygen vacancies content. Indeed, the oxygen vacancy content clearly declines with increasing particle size as found with Raman spectroscopy (Fig. 3) which is in accordance with results reported by various research groups for small mono-size ceria particles (<10 nm), thin ceria films and La^{3+}, Pr^{3+} doped ceria particles studied by Raman spectroscopy [47–49].

Fig. 6 shows the integrated intensity of the oxygen displacement band (258 cm^{-1}) in the Raman spectra as a function of BET

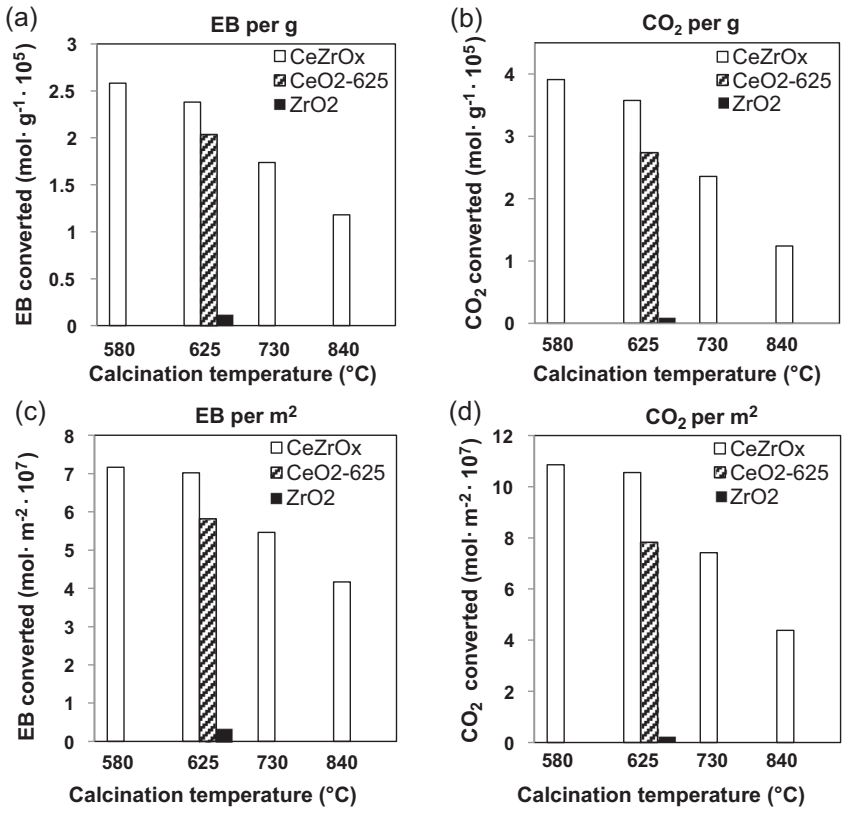

Fig. 5. EB conversion per g (a) and m^2 (c) and CO_2 conversion per g (b) and m^2 (d) for the $CeZrO_x$ catalysts, pure CeO_2 and monoclinic ZrO_2. Reaction conditions: $T = 560\,^{\circ}C$, $F = 30\,ml\,min^{-1}$, CO_2:EB = 7, m_{cat} = 27–49 mg.

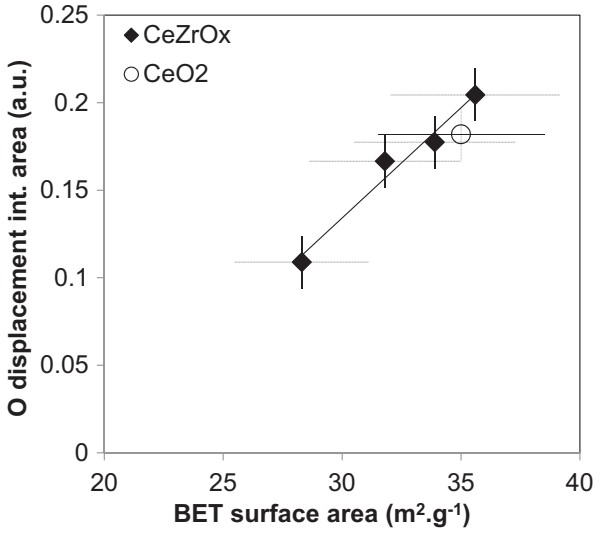

Fig. 6. BET surface area versus integrated intensity of the oxygen displacement band at 258 cm^{-1} in the Raman spectra of $CeZrO_x$ and CeO_2-625 catalysts.

surface area. The band at 258 cm^{-1} was taken as a measure for the concentration of vacancies since it was found that the formation of vacancies is associated with oxygen displacement in the lattice as a result of carbonate formation on the surface [50]. Clearly, the amount of oxygen displacement is linearly related to the BET surface area for the $CeZrO_x$ catalysts, consistent with the increase of particle size and shape change. In Fig. 6, the undoped CeO_2-625 sample deviates only slightly from the linear relation between the Zr-doped samples. This suggests that the addition of a low amount of zirconia (Ce:Zr = 92:8 molar ratio) only has a minor effect on the oxygen displacement and corresponding oxygen vacancy concentration after calcination at temperatures between 580 and 840 °C. The results are consistent with literature reporting decreasing oxygen vacancy concentration for ceria upon calcination [36]. For solid solutions of zirconia and ceria with zirconia concentration up to 40 mol% a stabilizing effect was reported [32]. However, our samples have been prepared with much lower zirconia content, and Raman spectroscopy results (Fig. 3) indicated that not all zirconia was incorporated in the lattice, thus the stabilizing effect of zirconia can be considered minor for these samples.

4.2. The effect of calcination temperature on ethylbenzene dehydrogenation with CO_2

All catalysts showed a strong deactivation in the first hour of the experiment (Fig. 4a and Fig. 1 in supplementary information). In the same period a clear increase in styrene selectivity was observed, while the amount of produced benzene decreased (Fig. 4b and Fig. 1 in supplementary information). The strong deactivation of the catalysts could be due to the consumption of active lattice oxygen, which results in an over-oxidation of EB resulting in benzene in addition to styrene. Further, the presence of coke, as confirmed by TGA on the spent catalysts, is an additional possible explanation for the deactivation of the catalysts. The participation of lattice oxygen species in EB dehydrogenation has been reported by several research groups, for vanadia and perovskite based catalysts [51–53]. To regenerate these sites an oxidant is added to the reactant, often steam or molecular oxygen. In the present study, CO_2 was added instead as a soft oxidant, however, the strong deactivation shows that CO_2 is not able to recover the active oxygen species at the speed of consumption.

The decreasing CO_2 conversion in the first hour (Fig. 4a) cannot be due to adsorption by ceria since the samples were first

stabilized in CO_2. The deactivation pattern is identical to that of EB conversion, pointing to a relation between the reactions of these molecules. At all times, the ratio of [mol CO_2 converted/mol CO produced] was close to 1, indicating a reduction of CO_2. In addition, the amount of H_2 detected was always lower than the amount of styrene produced. After deactivation, about 60% of H_2, based on styrene formation, was converted. The disappearance of hydrogen suggests additional pathways like CO_2 dissociation and subsequent production of water from H_2 and surface oxygen as has been proposed in the literature [18,21]. Alternatively, H_2 could react with CO_2 as in the reverse water gas shift reaction, as has been proposed by others [23,24]. Unfortunately, we were not able to quantify the amounts of water produced. The exact details of the first stage of the reactions and the effect of CO_2 on the conversion of EB are, however, beyond the scope of this paper, and will be discussed in a paper currently in preparation [54].

Here we focus on the activity of the catalyst at steady-state, i.e. after the strong deactivation in the first hour. It should be noted that TOS still is relatively short compared to other studies in literature in which additional active sites due to coke formation were proposed [20]. After consumption of lattice oxygen, ethylbenzene could be converted via non-oxidative dehydrogenation as has been proposed before [33,34].

In Fig. 5a and b, at first sight, the decreasing EB and CO_2 conversion per gram of catalyst with higher calcination temperature can be related to the decreasing surface area. However, Fig. 5c and d clearly shows that the EB and CO_2 conversion per m^2 also decreased with increasing calcination temperature. Consequently, the explanation for the decreasing activity must be more complex than only a decrease in surface area. Similarly, the OSC capacity of polycrystalline ceria calcined at different temperatures was also found not to be directly related with BET surface area [16].

Reduced catalytic activity of the samples calcined at higher temperatures is in accordance with results reported for mesoporous ceria in oxidative EBDH [15]. The authors proposed that the superior catalytic performance of small ceria crystallites originated from their enhanced redox capacity. According to [55] mesostructured ceria exhibited higher surface area and enhanced redox capacity. The enhanced redox capacity will be determined by the number of defect sites as well as the reactivity of those sites, as was found for EB conversion in the presence of N_2O over reactive ceria [16]. The Raman spectra in Fig. 3 suggest that the higher catalytic activity for smaller $CeZrO_x$ particles could be related to an increasing number of oxygen deficient domains. Fig. 6 showed that the amount of displaced oxygen is linearly related to the BET surface area.

Fig. 7 shows the EB conversion per m^2 as a function of oxygen displacement integrated intensity as determined with Raman spectroscopy. Although the Raman experiments were performed ex situ in air, the conditions for all samples were identical. This allows for comparison with the observed catalytic activity of the samples, although it is not a representation of the real number of oxygen vacancies at reaction conditions, which will be determined by the pre-treatment and reaction conditions. In situ Raman experiments would be needed to further confirm this correlation.

The increasing activity per m^2 with increasing amount of oxygen vacancies in Fig. 7 points to an altered reactivity of the vacancies affecting the conversion rate of EB and CO_2. The inclusion of the pure CeO_2-625 sample in the linear relation in Fig. 7 shows that the observed relationship also holds for samples without zirconia.

The observed relation can be explained by the shape change of the particles upon calcination (Fig. 1). The alteration from small cubic shaped to larger and more spherical particles increases the exposure of (1 1 1) surface planes. The (1 1 1) structure is known to have a lower oxygen vacancy stability than (1 0 0) planes in ceria cubes [37,50,56,57]. This observation is similar to a recent study reporting on the relation between the reactivity of lattice oxygen

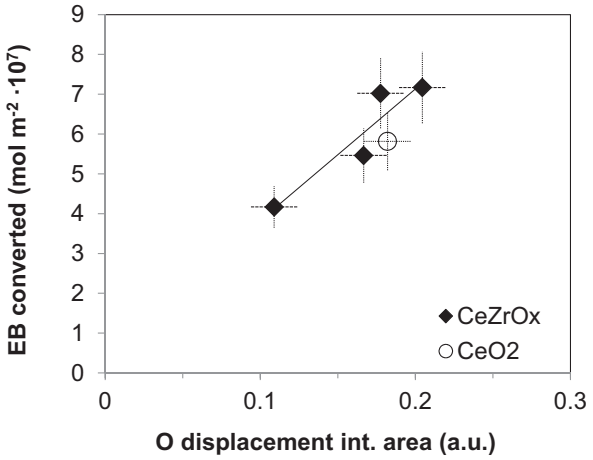

Fig. 7. Catalyst activity vs. integrated intensity of the oxygen displacement band at 258 cm^{-1} in the Raman spectra of $CeZrO_x$ and CeO_2-625 catalysts.

sites in perovskite catalysts with styrene formation rates from EB in the presence of steam [53]. In other words, not only the number of oxygen vacancies decreases with increasing particle size due to a lower surface area, but also their reactivity decreases because of the altered size and shape. This in turn affects the observed EB and CO_2 conversion rates. These results imply that the reducibility of ceria defined by both crystallite size and geometry influences the rate of EB dehydrogenation as well as the RWGS reaction. In a following paper the relation between these two reactions over ceria is further investigated [54].

5. Conclusion

Calcination of $CeZrO_x$ at different temperatures, resulted in a series of catalysts with different morphology and particle size as observed with HRSEM and XRD. Raman spectroscopy revealed annihilation of oxygen vacancies, i.e. oxygen displacement sites with increasing calcination temperature. The activity expressed in mol m^{-2} for ethylbenzene dehydrogenation to styrene in the presence of CO_2 depended not only on the amount but also on the specific reactivity of lattice defects sites, which was determined by the size and shape of the particles.

Acknowledgements

This work was performed under the auspices of NIOK, the Netherlands Institute of Catalysis Research. Financial support of ASPECT Project No. 05362021 is greatly acknowledged.

We thank to Ing. L. Vrielink for BET measurements and Drs. M. Smithers for HRSEM measurements. Technical support of Ing. B. Geerdink and K. Altena is highly appreciated.

Appendix A. Supplementary data

Supplementary material related to this article can be found, in the online version, at http://dx.doi.org/10.1016/j.apcata.2013.09.010.

References

[1] G. Eranna, B.C. Joshi, D.P. Runthala, R.P. Gupta, Crit. Rev. Solid State Mater. Sci. 29 (2004) 111–188.
[2] N. Izu, W. Shin, N. Murayama, S. Kanzaki, Sens. Actuators B 87 (2002) 95–98.
[3] J.-H. Wang, M. Liu, M.C. Lin, Solid State Ionics 177 (9–10) (2006) 939–947.
[4] S.C. Singhal, Mater. Res. Bull. 25 (3) (2000) 16–21.
[5] T. Kudo, H.H. Obayashi, J. Electrochem. Soc. 122 (1) (1975) 142–147.

[6] A. Corma, P. Atienzar, H. García, J.-Y. Chane-Ching, Nat. Mater. 3 (2004) 394–397.
[7] A.Z. Turković, Z.C. Orel, Sol. Energy Mater. Sol. Cells 45 (1997) 275–281.
[8] M. Luo, J. Chen, L. Chen, J. Lu, Z. Feng, C. Li, Chem. Mater. 13 (2001) 197–202.
[9] T. Masui, Y. Peng, K. Machida, G. Adachi, Chem. Mater. 10 (1998) 4005–4009.
[10] R.H. Nibbelke, M.A.J. Campman, J.H.B.J. Hoebink, G.B. Marin, J. Catal. 171 (1997) 358–373.
[11] P. Ratnasamy, D. Srinivas, C.V.V. Satyanarayana, P. Manikandan, R.S. Senthil Kumaran, M. Sachin, V.N. Shetti, J. Catal. 221 (2004) 455–465.
[12] N. Yi, R. Si, H. Saltsburg, M. Flytzani-Stephanopoulos, Energy Environ. Sci. 3 (2010) 831–837.
[13] R. Si, M. Flytzani-Stephanopoulos, Angew. Chem. Int. Ed. 47 (2008) 2884–2887.
[14] T. Staudt, Y. Lykhach, N. Tsud, T. Skála, K.C. Prince, V. Matolín, J. Libuda, J. Catal. 275 (2010) 181–185.
[15] J. Xu, L.-C. Wang, Y.-M. Liu, Y. Cao, H.-Y. He, K.-N. Fan, Catal. Lett. 133 (2009) 307–313.
[16] B. Murugan, A.V. Ramaswamy, J. Am. Chem. Soc. 129 (2007) 3062–3063.
[17] F. Cavani, F. Trifiro, Appl. Catal. A Gen. 133 (1995) 219–239.
[18] M.B. Ansary, S.-E. Park, Energy Environ. Sci. 5 (2012) 9419–9437.
[19] M.-O. Sugino, H. Shimada, T. Turuda, H. Miura, N. Ikenaga, T. Suzuki, Appl. Catal. A Gen. 121 (1995) 125–137.
[20] N. Mimura, I. Takahara, M. Saito, T. Hattori, K. Ohkuma, M. Ando, Catal. Today 45 (1998) 61–64.
[21] J.-S. Chang, S.-E. Park, M.S. Park, Chem. Lett. 26 (1997) 1123–1124.
[22] T. Badstube, H. Papp, P. Kustrowski, R. Dziembaj, Catal. Lett. 55 (1998) 169–172.
[23] A.L. Sun, Z.F. Qin, J.G. Wang, Appl. Catal. A Gen. 234 (2002) 179–189.
[24] Y. Sakurai, T. Suzaki, N. Ikenaga, T. Suzuki, Appl. Catal. A Gen. 192 (2000) 281–288.
[25] Y. Sakurai, T. Suzaki, K. Nakagawa, N. Ikenaga, H. Aota, T. Suzuki, J. Catal. 209 (2002) 16–24.
[26] N. Ikenaga, T. Tsuruda, K. Senma, T. Yamaguchi, Y. Sakurai, T. Suzuki, Ind. Eng. Chem. Res. 39 (2000) 1228–1234.
[27] C. Nederlof, F. Kapteijn, M. Makkee, Appl. Catal. A Gen. 417–418 (2012) 163–173.
[28] B.M. Reddy, D.-S. Han, N. Jiang, S.-E. Park, Catal. Surv. Asia 12 (2008) 56–69.
[29] D.R. Burri, K.-M. Choi, J.-H. Lee, D.-S. Han, S.-E. Park, Catal. Commun. 8 (2007) 43–48.
[30] A. Trovarelli (Ed.), Catalysis by Ceria and Related Materials, Imperial College Press, London, 2002, pp. 1–528.
[31] J.A. van Bokhoven, ChemCatChem 1 (2009) 363–364.
[32] E. Mamontov, T. Egami, R. Brezny, M. Koranne, S. Tyagi, J. Phys. Chem. B 104 (2000) 11110–11116.
[33] G. Balducci, M.S. Islam, J. Kaspar, P. Fornasiero, M. Graziani, M. Saiful, J.D. Gale, J. Phys. Chem. B 101 (1997) 1750–1753.
[34] G. Balducci, J. Kaspar, P. Fornasiero, M. Graziani, M. Saiful Islam, D. Julian, Gale, J. Phys. Chem. B 101 (1997) 1750–1753.
[35] G. Balducci, P. Fornasiero, R. Di Monte, J. Kaspar, S. Meriani, M. Graziani, Catal. Lett. 33 (1995) 193–200.
[36] R. Si, Y.W. Zhang, S.J. Li, B.X. Lin, C.H. Yan, J. Phys. Chem. B 108 (2004) 12481–12488.
[37] M. Baudin, M. Wojcik, K. Hermansson, Surf. Sci. 468 (2000) 51–61.
[38] K. Zhou, X. Wang, X. Sun, Q. Peng, Y. Li, J. Catal. 229 (2005) 206–212.
[39] K.B. Chen, W.B. Chen, S.F. Weng, C.S. Lee, M.C. Lin, J. Phys. Chem. C 113 (2009) 5031–5034.
[40] G.N. Vayssilov, M. Mihaylov, P.S. Petkov, K.I. Hadjiivanov, K.M. Neyman, J. Phys. Chem. C 115 (2011) 23435–23454.
[41] S. Meriani, G. Spinolo, Powder Diffr. 2 (4) (1987) 255–256.
[42] B.M. Reddy, P. Lakshmanan, A. Khan, C. López-Cartes, T.C. Rojas, A. Fernández, J. Phys. Chem. B 109 (2005) 1781–1787.
[43] J.E. Spanier, R.D. Robinson, F. Zhang, S.-W. Chan, I.P. Herman, Phys. Rev. B 64 (2001) 245407–245408.
[44] Z. Wu, M. Li, J. Howe, H.M. Meyer III, S.H. Overbury, Langmuir 26 (2010) 16595–16606.
[45] J.-M. Costantinia, A. Kahn-Harari, F. Beuneu, F. Couvreur, J. Appl. Phys. 99 (2006) 123501–123507.
[46] J.-N. Park, J. Noh, J.-S. Chang, S.-E. Park, Catal. Lett. 65 (2000) 75–78.
[47] F. Zhang, S.-W. Chan, J.E. Spanier, E. Apak, Q. Jin, R.D. Robinson, I.P. Herman, Appl. Phys. Lett. 80 (2002) 127–129.
[48] J.L.M. Rupp, B. Scherrer, L.J. Gauckler, Phys. Chem. Chem. Phys. 12 (2010) 11114–11124.
[49] S. Patil, S. Seal, Y. Guo, A. Schulte, J. Norwood, Appl. Phys. Lett. 88 (2006) 243110–243113.
[50] M. Nolan, G.W. Watson, J. Phys. Chem. B 110 (2006) 16600–16606.
[51] K. Saito, K. Okuda, N.O. Ikenaga, T. Miyake, T. Suzuki, J. Phys. Chem. A 114 (11) (2010) 3845–3854.
[52] D.-Y. Hong, V.P. Vislovskiy, S.-E. Park, M.-S. Park, J.S. Yoo, J.-S. Chang, Bull. Korean Chem. Soc. 26 (2005) 1743–1748.
[53] R. Watanabe, Y. Sekine, J. Kojima, M. Matsukata, E. Kikuchi, Appl. Catal. A Gen. 398 (2011) 66–72.
[54] M. Kovacevic, L. Lefferts, B.L. Mojet, in preparation.
[55] F. Giordano, A. Trovarelli, C. De Leitenburg, M. Giona, J. Catal. 193 (2000) 273–282.
[56] E. Aneggi, J. Llorca, M. Boaro, A. Trovarelli, J. Catal. 234 (2005) 88–95.
[57] T.X.T. Sayle, S.C. Parker, C.R.A. Catlow, Surf. Sci. 316 (1994) 329–336.